Control of aragonite deposition in colonial corals by intra-skeletal macromolecules

Giuseppe Falini [a,*], Michela Reggi [a], Simona Fermani [a], Francesca Sparla [b], Stefano Goffredo [c], Zvy Dubinsky [d], Oren Levi [d], Yannicke Dauphin [e,*], Jean-Pierre Cuif [e]

[a] Dipartimento di Chimica 'G. Ciamician', via Selmi 2, Alma Mater Studiorum, Università di Bologna, 340126 Bologna, Italy
[b] Dipartimento di Farmacia e Biotecnologie, via Irnerio 42, Alma Mater Studiorum, Università di Bologna, 340126 Bologna, Italy
[c] Dipartimento di Scienze Biologiche, Geologiche e Ambientali, via Selmi 3, Alma Mater Studiorum, Università di Bologna, 340126 Bologna, Italy
[d] The Mina and Everard Goodman Faculty of Life Sciences, Bar Ilan University, Ramat Gan, Israel
[e] Université Paris-Sud, Orsay, Bat. 504, UMR IDES, F-91405 Orsay, France

ARTICLE INFO

ABSTRACT

Scleractinian coral skeletons are composed mainly of aragonite in which a small percentage of organic matrix (OM) molecules is entrapped. It is well known that in corals the mineral deposition occurs in a biological confined nucleation site, but it is still unclear to what extent the calcification is controlled by OM molecules. Hence, the shape, size and organization of skeletal crystals from the fiber level through the colony architecture, were also attributed to factors as diverse as nucleation site mineral supersaturation and environmental factors in the habitat. In this work the OMs were extracted from the skeleton of three colonial corals, *Acropora digitifera*, *Lophelia pertusa* and *Montipora caliculata*. *A. digitifera* has a higher calcification rate than the other two species. OM molecules were characterized and their $CaCO_3$ mineralization activity was evaluated by experiments of overgrowth on coral skeletons and of precipitation from solutions containing OM soluble and insoluble fractions and magnesium ions. The precipitates were characterized by spectroscopic and microscopic techniques. The results showed that the OM molecules of the three coral share similar features, but differ from those associated with mollusk shells. However, *A. digitifera* OM shows peculiarities from those from *L. pertusa* and *M. caliculata*. The $CaCO_3$ overgrowth and precipitation experiments confirm the singularity of *A. digitifera* OM molecules as mineralizers. Moreover, their comparison indicates that only specific molecules are involved in the polymorphism control and suggests that when the whole extracted materials are used the OM's main effect is on the control of particles' shape and morphology.

1. Introduction

Scleractinia corals possess several records in terms of their mineralization activity. They represent the biggest source of biogenic calcium carbonate (Spalding et al., 2001; Cohen and McConnaughey, 2003) and they are among the fastest marine mineralizing organisms (Marshall and Clode, 2004). Despite their great relevance in biomineralization, and the plethora of articles published in this field (Tambutté et al., 2011 and references therein), many aspects of their mechanism of mineralization are still a source of discussions and controversies. The main issue is the relative level of biological and environmental control over calcification.

It has long been recognized that coral skeletons comprise both inorganic (aragonite) and organic components (e.g. Wilfert and Peters, 1969; Young, 1971), but the main issue is the relative level of biological and environmental control over calcification. In geochemical research area, opinions inspired by the spherulitic crystallization model (Bryan and Hill, 1941) are still prevalent. If presence of an organic component has become accepted, its active role in the biomineralization process is still considered doubtful (Holcomb et al., 2009). Among biologists, organic components entrapped within coral skeletons are usually referred to as "organic matrices (OM)" and owing to an unusual amino-acid composition (high concentrations of acidic amino acids) have been suggested to play an important role in the coral mineralization process (Mitterer, 1978; Constantz and Weiner, 1988; Goffredo et al., 2011). Morphology of coral colonies are dramatically affected by habitat conditions (Jokiel, 1978), nevertheless the changes always remain within the species-specific "vocabulary" controlled by the taxon's DNA (Cuif et al., 2003a).

* Corresponding authors. Fax: +33 (0)1 69 15 61 23 (Y. Dauphin), +39 051 2099456 (G. Falini).
E-mail addresses: giuseppe.falini@unibo.it (G. Falini), yannicke.dauphin@u-psud.fr (Y. Dauphin).

Regarding the fine scale features of coral skeletons, structural analysis has long been carried out by using optical microscope with polarized light. This led to valorization of the "sclerodermite" as the microstructural unit of the skeletons: a group of radiating fibers with crystal-like appearance (Ogilvie, 1896; Wells, 1956). However, investigations conducted by scanning electron microscopy, microprobe analysis and synchrotron-based mapping (Cuif and Dauphin, 1998) have clearly established that the actual building unit of the skeleton is a few micrometer thick, mineralizing growth layer, synchronically produced for a given septa. This repeatedly produced unit comprises two distinct areas with specific modes of mineralization (Fig. 1). At the growing edge of the septa the mineral phase is in the form of tiny randomly oriented crystals, deposited at the top of the septal spines or growing edge with species-specific geometry, chemical and isotopic signatures. These distal structures, producing the septal framework, are then covered by the successive mineral layers which progressively create the fibers (i.e. constituting the major part of the corallite structure).

The biochemical composition of the organic compounds associated with the mineral units are essentially known from numerous analyses carried out on the organic components extracted from coral skeletons after decalcification and purification processes. From Young (1971) to Constantz and Weiner (1988) proteins and glycosaminoglycans but also sulfated polysaccharides (Dauphin, 2001; Cuif et al., 2003b) have been consistently found in the skeletons of the numerous species covering the whole taxonomic diversity of the phylum. Lipids are also present in the OM (Farre et al., 2010).

However, the mode of action of these organic compounds is still debatable. Initial models favored the "template mechanism" in which organic layers were acting as a scaffold for Ca-carbonate oriented crystallization. In contrast to models involving a liquid layer with chemical properties close to sea-water (McConnaughey and Whelan, 1997; Adkins et al., 2003) as the place where crystallization occurs, Clode and Marshall (2002) have established the existence of direct contact between cells and skeleton. Calcification occurs within a gel secreted, or a high viscous sol, at the interface between the calicoblastic cells and the skeleton. In situ XANES mapping of organic components (proteins and sulfated polysaccharides) have shown that organic and mineral components were not distributed among alternating layers, but associated within each growth layer at a submicrometer scale (Cuif et al., 2003b).

Molecular models suggest formation of a glycoproteic architectural framework bearing sites for development of a crystalline structure (Addadi et al., 2006). More recently attention was drawn to the potential role of OMs as carriers of the mineral component, possibly in amorphous status, crystallization itself trapping the organic phases along the boundaries of the grains (Cuif et al., 2008; Weiner and Addadi, 2011; Motai et al., 2012). This model is supported by $CaCO_3$ crystallization experiments in gel and partial gels (Asenath-Smith et al., 2012).

The real role of the OM in the dynamics of skeleton formation of corals is enigmatic and is related to the information on its properties once extracted from the skeleton. However, bearing in mind these limits, but supported by many analogous studies on mollusk shells, it has been recently demonstrated, by in vitro studies, that the OM from a coral species (Balanophyllia europaea) influences the polymorphism and morphology of $CaCO_3$ (Goffredo et al., 2011).

Here, we extended this study to different species of colonial corals, Montipora caliculata, Acropora digitifera (French Polynesia) and Lophelia pertusa (Atlantic Ocean), living in different habitats and having diverse calcification rates. Respectively, first and second largest coral genus in the present-day seas with respect to taxonomical diversity, Acropora and Montipora belong to the most suc-

cessful and most studied coral family Acroporidae. According to Veron (2000), Acroporidae and Caryophyllidae (the Family to which the deep-sea coral Lophelia belongs) are distributed into two major supra-ordinal lineages, possibly distinct since the Triassic times. The aim of the present study is to determine whether the OM extracted from different corals shows a different capability to interact with $CaCO_3$ and if this is related with the coral species.

2. Results

2.1. Skeletal structures in corals

Scanning electron microscope (SEM) images of the studied species showed the common structural pattern of the coral skeleton (Fig. 1): the early mineralization zone (EMZ) was composed of small rounded granules. EMZs were more sensitive to etching than the fibers (Cuif and Dauphin, 2005). Then, fibers were produced with a rhythmic growth. Growth layers are about 2–3 μm thick. However, the size and arrangement of EMZ and fibers depend upon the species (Fig. 1a, b, f, j). The inner structure of EMZ and fibers becomes visible using atomic force microscopy. Both EMZ and fibers are composed of rounded small granules (Fig. 1d, g–i, k, l). These granules are surrounded by a cortex, the exact nature of which remains still unknown. Nevertheless, from phase image contrast, it can be said that the cortex is probably a mixture of organic and amorphous components. The inner part of the granules is also heterogeneous, as shown by the changes in colors in phase images.

2.2. Studies on the intra-skeletal organic matrix

In M. caliculata, A. digitifera and L. pertusa the OM was embedded in a skeleton of pure aragonite, as shown by the X-ray powder diffraction patterns (Fig. 1SI). A first quantification of the OM content in the skeleton was carried out by thermogravimetric analysis (TGA). The skeletons' thermograms showed a first weight loss in a range around 150–220 °C followed by one between about 280 and 450 °C (Fig. 2SI). The total weight loss (water + OM; see Cuif et al., 2004) was of 3.4 ± 0.1 $(0.9 \pm 0.1 + 2.5 \pm 0.1)$, 2.7 ± 0.1 $(1.0 \pm 0.1 + 1.7 \pm 0.1)$ and 3.9 ± 0.1 $(1.3 \pm 0.1 + 2.6 \pm 0.1)$ % (w/w) in M. caliculata, A. digitifera and L. pertusa, respectively. The OM concentration was also determined after acetic acid extraction from the skeleton. This material, formed by the soluble (SOM) and insoluble (IOM) fractions of OM, was about 0.3, 0.2 and 0.1% (w/w) in M. caliculata, A. digitifera and L. pertusa, respectively. The quantification of the relative amount of the OM fractions, SOM and IOM, was a difficult task, since a significant variability was observed from one extraction to another. However, as the result of six extractions the mass ratio between SOM and IOM was roughly estimated to be 1.4 in M. caliculata, 5.0 in A. digitifera, and 1.5 in L. pertusa.

The chemical–physical characterization of the OM fractions was performed by Fourier transform infrared spectroscopy (FTIR), polyacrylamide gel electrophoresis (SDS–PAGE) and amino-acidic analyses (AAA). Table 1 summarizes the observations from the FTIR spectra of SOM and IOM obtained from six extraction processes from different coral skeletons of each species. In Fig. 2 the most representative spectra are shown. In general SOM and IOM showed the same absorption bands, regardless of the coral species; however, differences were observed in their relative intensities, and to a minor extent in their maxima. Two marked bands at about 2920 cm^{-1} and 2851 cm^{-1} and a weak one at 1737/35 cm^{-1} were observed in all fractions. In the SOMs the amide I bands were centered around 1654 cm^{-1}, this band partially shifted towards lower wavenumbers, around 1636 cm^{-1}, in the IOMs. The amide II band, at around 1542 cm^{-1}, was weak with respect to the amide I band, in both SOM and IOM, particularly in M. caliculata. The band at
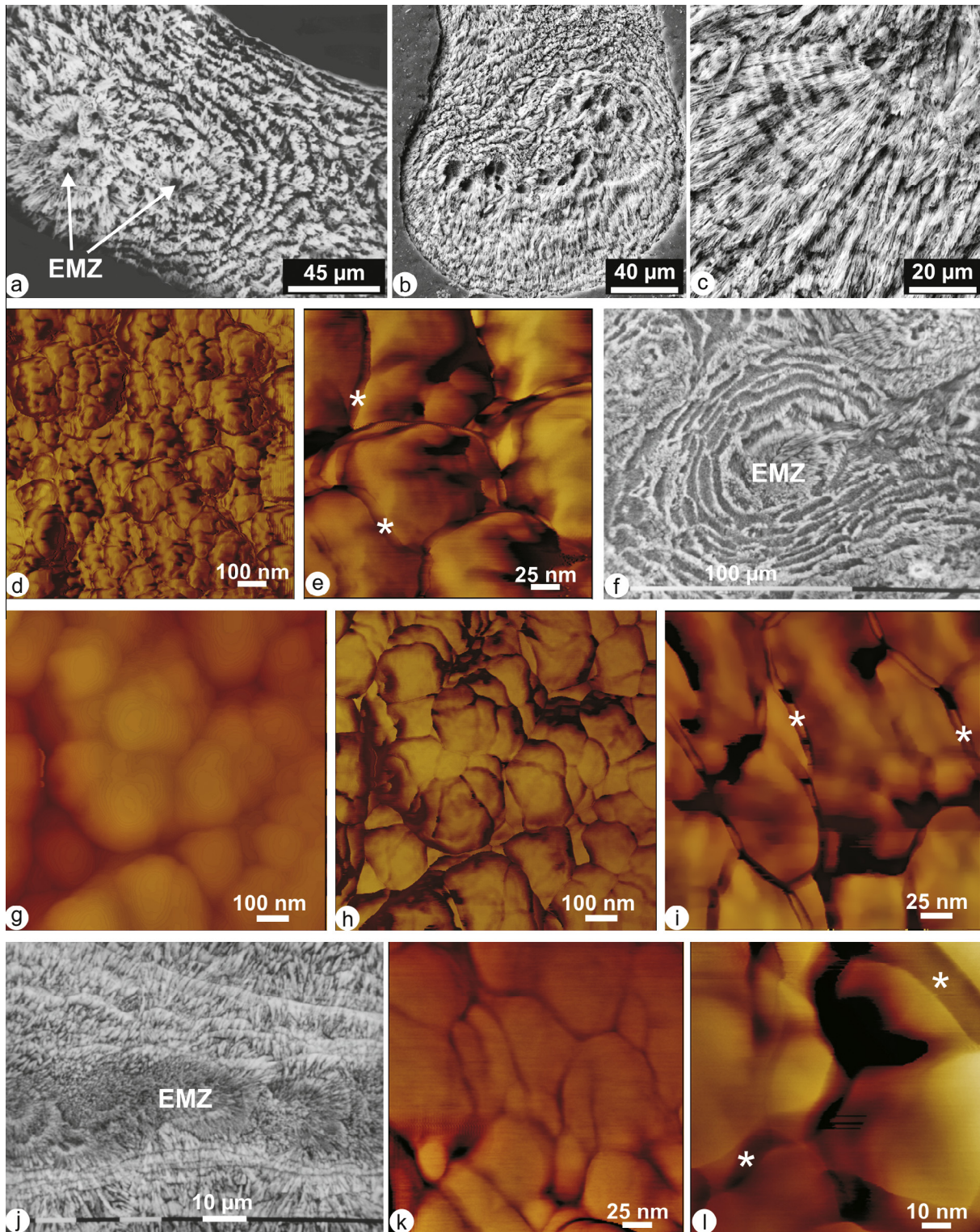
Fig.1. a–e: *M. caliculata*. Etching clearly shows the dual structure of coral skeletons: the superposed growth layers (a–b) cover the framework built by the small round shaped units which are formed at the tip of the skeletal units (EMZ: early mineralization zones); c: etching also demonstrates the coordinated stepping growth mode of fibers; d–e: atomic force microscopy reveals the reticulate structure of the skeleton. a–c: Alcalase etching of polished sections; d–e: polished section, etched with formic acid (5%) and glutaraldehyde (0.1%) for 5 s. f–i: *A. digitifera*. f: A typical view of skeletal organization: instead of continuous and regularly superposed growth layer, EMZ are surrounded by densely packed digitiform units with a spiral mode of growth (EMZ); polished and etched section, formic acid 5% for 5 s. g: Detail of the granular structure shown by AFM (polished and etched section) g: height image, polished section, etched with formic acid (5%) and glutaraldehyde (0.1%) for 5 s. h: Phase image of the same, i: same sample, granules surrounded by a thin cortex (*) of organic matrix ± ACC, AFM phase image. j–l: *L. pertusa*. j: typical for this genus is the wide EMZ median of the septa, covered by regular layers forming fibers; polished and etched section (HCl 1% for 5 s). k–l: Both domains are built by a reticulate composite material, with round shaped mineral units covered by a non crystallized phase strongly interacting with AFM probe tip (*). Polished sections, etched with formic acid (5%) and glutaraldehyde (0.1%) for 5 s.

around 1460 cm^{-1} was well defined in the IOM but weak in the SOM from all the species. An opposite trend was observed for the band at about 1460 cm^{-1}, which was more evident in SOM than IOM, except that in the IOM from *L. pertusa*. The band around

Table 1
Main absorption bands in the FTIR spectra of soluble (SOM) and insoluble (IOM) OM fractions extracted from the skeleton of *A. digitifera* (*AD*), *M. caliculata* (*MC*) and *L. pertusa* (*LPE*). Their relative intensity is indicated in brackets; strong (*s*), medium (*m*) or weak (*w*).

	SOM			IOM		
	MC	*AD*	*LPE*	MC	*AD*	*LPE*
CH stretching	2920 (*s*)	2920 (*s*)	2922 (*s*)	2919 (*s*)	2920 (*s*)	2922 (*s*)
CH stretching	2851 (*m*)	2851(*m*)	2851/4 (*m*)	2851 (*m*)	2851 (*m*)	2852 (*m*)
Carboxylic stretching	1735 (*w*)	1735 (*w*)	1736 (*w*)	1735 (*w*)	1732/7[*] (*w*)	1737 (*w*)
Amide I (α-helix, r.c.)	1655 (*s*)	1650/55 (*s*)	1655 (*s*)	1652 (*w*)	1650 (*w*)	1653 (*m*)
Amide I (β-sheet)	1637 (*w*)	1637 (*w*)	1639 (*w*)	1639 (*s*)	1632/8 (*s*)	1639 (*s*)
Amide II	1540/7 (*w*)	1542 (*w*)	1542 (*m*)	1544 (*w*)	1542 (*w*)	1545 (*w*)
CH$_2$ bending	1457/63 (*w*)	1459 (*m*)	1456/62 (*w*)	1457/63 (*m*)	1465 (*m*)	1460 (*m*)
Carboxylate stretching	1429 (*m s*)	1420/31 (*m*)	1420 (*m*)	1428/32 (*w*)	1422/8 (*w*)	1420 (*w*)
CH$_3$ bending	1384 (*w*)	1385 (*m*)	1384 (*m*)	1385 (*w*)	1384 (*w*)	1384 (*w*)
sugar groups[**]	1074/7 (*s*)	1080 (*s*)	1073/8 (*s*)	1060/80 (*s*)	1078 (*s*)	1079 (*s*)

[*] Two values are reported to indicate that this band maximum appeared in one of the two positions among different extraction products.

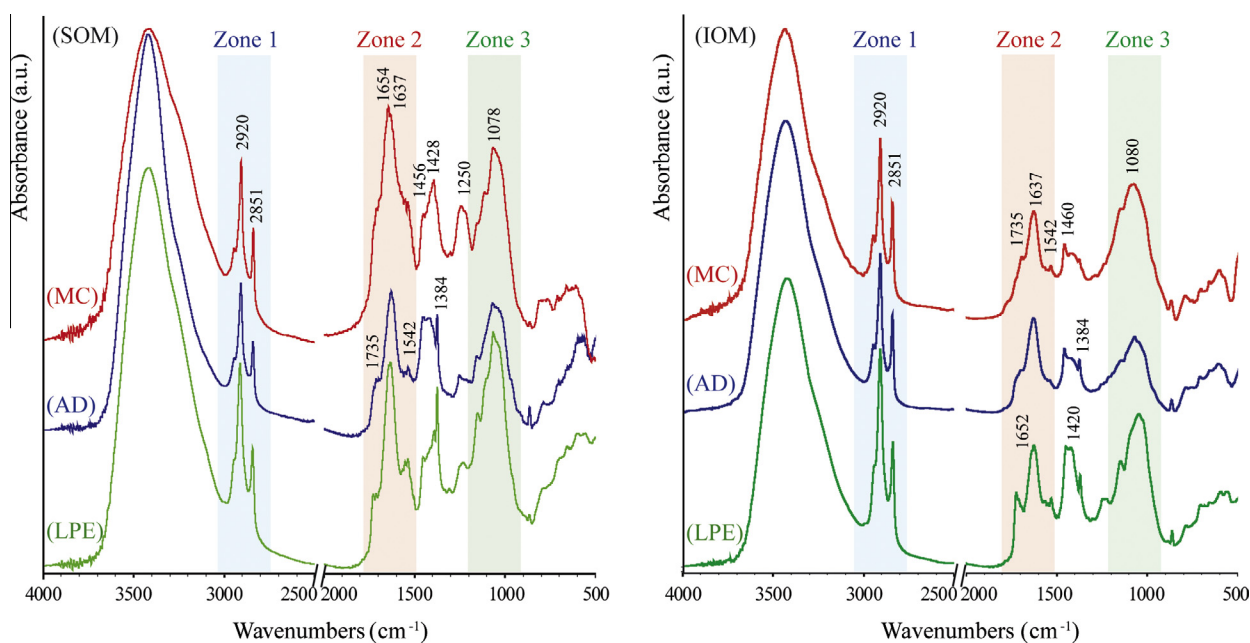[**] The sugar groups region absorption presents several bands, here the most intense one is reported.

Fig.2. FTIR spectra of intra-skeletal soluble (SOM) and insoluble (IOM) organic matrix extracted from the aragonitic skeleton of *A. digitifera* (*AD*), *M. caliculata* (*MC*) and *L. pertusa* (*LPE*). The maximum of the absorption bands are indicated. The three zones define diagnostic regions of functional groups which could be mainly associated to the presence of lipids (zone 1), protein and polysaccharides (zone 2) and polysaccharides (zone 3).

1250 cm^{-1} was evident only in the SOM from *M. caliculata*. The bands in the region between 1080 and 1030 cm^{-1} were observed in the spectra of all the extracts. To estimate the relative amounts of the main functional groups of the OM from the FTIR spectra, three zones (1–3) were defined (Fig. 2, Table 1SI). In the zone 1 (3000–2800 cm^{-1}) the absorption bands due to the methylene and methyl groups' vibration modes were present, they could mainly be related to the presence of fatty acids, mainly in IOM, or to molecules bearing alkylic chain regions. In the zone 2 (1750–1500 cm^{-1}) were located the absorption bands mainly associable to the amide I and II vibration modes of proteins (and of some sugars). In zone 3 (1100–950 cm^{-1}) ether bonds and C–C single bond vibration modes, mainly associable to polysaccharides, were present (Parker, 1983). The integrated intensities of the absorption zones 1 and 3 were normalized to that of zone 2 (Table 1SI). Then a Mann–Whitney statistical test was carried out to verify if the differences in the relative zone absorption intensities between SOM and IOM of the same species and among different species were significant. In the SOM from *A. digitifera* and *M.*

caliculata significant lower relative absorption intensity in the zone 1 with respect to IOM was observed. In the comparison among OM fractions from different species only the SOM from *L. pertusa* showed a significant higher absorption in zone 3.

The macromolecules comprising SOM fractions were also investigated by SDS–PAGE (Fig. 3). *L. pertusa* SOM was characterized by the presence of many bands, gathered around 65, 43 and 35 kDa. *M. caliculata* showed two weak bands at 64 and 41 kDa. In *A. digitifera* no bands were detected. The PAS stain did not underline glycoprotein in any of the species. The AAA from SOM and IOM was reported in Table 2. SOM was always characterized by a higher content of aspartic (and asparagine) acidic residues than that of IOM. In *L. pertusa* the difference in aspartic residue content between SOM and IOM was lower than in the other two species. The content of hydrophobic residues, Gly, Ala, Val, Ile and Leu, was always higher in IOM (43–51 mol%) than in SOM (19–30 mol%). The calculated average protein pIs (Sillero and Ribeiro, 1989) show that OMs were acidic, and IOM was less acidic than the SOM within a species (Fig. 3SI).
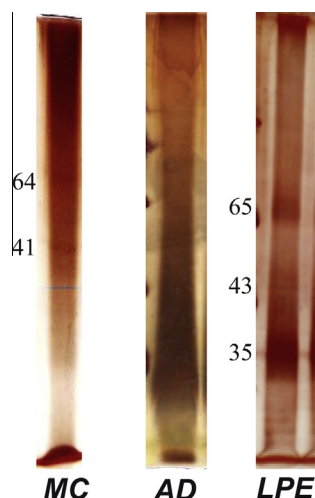
Fig.3. SDS–PAGE of intra-crystalline SOM extracted from the aragonitic skeleton *A. digitifera* (*AD*), *M. caliculata* (*MC*) and *L. pertusa* (*LPE*). The side numbers indicate the molecular weight (kDa) of the silver stain marked bands. This dye did not express any band from the SOM of *A. digitifera*.

Table 2
Amino acids composition (mol%) of soluble (SOM) and insoluble (IOM) fractions of OM proteins extracted from the skeleton of *A. digitifera* (*AD*), *M. caliculata* (*MC*) and *L. pertusa* (*LPE*).

	SOM			IOM		
	AD	LPE	MC	AD	LPE	MC
Asx[#]	46.77	30.97	34.62	16.95	24.66	13.80
Glx[$]	2.38	3.71	3.62	2.42	3.31	5.69
Ser	6.09	6.91	5.62	0.46	6.46	6.93
Gly	14.16	16.59	21.92	25.28	30.27	21.76
His	5.13	8.26	3.47	0.76	1.15	4.70
Thr	4.90	6.97	6.02	6.38	2.47	5.17
Arg	6.71	7.04	6.34	6.16	3.69	4.64
Ala	1.17	6.35	4.14	9.24	7.41	9.01
Tyr	6.83	2.47	1.30	0.50	1.94	2.63
Cys	–[*]	–	–	–	–	–
Val	0.35	1.80	1.39	3.49	1.32	3.81
Met	–	–	–	–	–	–
Phe	2.43	1.65	2.29	0.87	–	7.34
Ile	1.72	2.29	2.83	5.86	1.84	4.39
Leu	1.35	2.90	2.53	7.31	6.14	6.89
Lys	–	2.08	3.92	14.31	9.33	3.25

[#] Indicates the sum of Asp and Asn.
[$] Indicates the sum of Glu and Gln.
[*] Not quantified.

2.3. Overgrowth of CaCO₃ onto coral skeleton sections

The results of the CaCO$_3$ overgrowth experiments onto coral skeleton cross sections are illustrated in Fig. 4. As substrate a surface section, normal to the oral-aboral axis, close to the growing tips, was used. The growing media was a 10 mM calcium chloride solution. CaCO$_3$ crystals were observed sticking onto the skeleton cross sections and outside them (on the surface of the embedding resin). The overgrowth of aragonite was always observed onto the surface of the skeletons. These crystals appeared as long hexagonal needles in different orientations, probably reflecting the orientation of the underlying fibers of aragonite. The average cross section of these prisms was about 2 μm for *L. pertusa* and *M. caliculata* and less than 1 μm for *A. digitifera*. Onto the coral skeleton of *L. pertusa* and *M. caliculata* calcite crystals were also observed. Outside the skeleton of *A. digitifera*, *L. pertusa* and *M. caliculata* the precipitation

of aggregates of needle-like crystals of aragonite (Fig. 4 *AD*2), of rhombohedral {104} calcite crystals (Fig. 4 *LPE*2) and of aragonite crystals and calcite crystals showing {hk0} and {104} faces (Fig. 4 *MC*2), respectively, was observed.

2.4. Precipitation of CaCO₃ in the presence of OM fractions and magnesium ions

In a first set of experiments the precipitation of CaCO$_3$ from 10 mM CaCl$_2$ solutions containing the OM fractions was studied. In the absence of OM only rhombohedral calcite crystals precipitated (Fig. 4SI). The presence of OM fractions changed the particles' morphology and the polymorphism of the precipitated CaCO$_3$. This presence induced also an inhibition of the precipitation and a reduction of average particle sizes (Fig. 5 and Table 3). Six crystallization experiments were carried out for each combination using different batches of OM components. The reported results summarize the observed trends (Table 2SI). The presence of SOM (c_s = 0.44 mg/mL) always induced an aggregation of the CaCO$_3$ particles (Fig. 5 SOM). In the presence of *M. caliculata* SOM peanut and dumbbell shaped aggregates were observed; these shapes appeared to be formed by the association of nanometric sub-particles (Fig. 5 SOM *MC*, inset). In the presence of *A. digitifera* SOM dumbbells and spherical aggregates were also observed, but differing from the previous case, these particles showed surfaces formed by stacked multilayers (Fig. 5 SOM *AD*, inset). In the presence of *L. pertusa* SOM many different shapes were observed. The most representative one was that of spherical particles formed by the aggregation of nanoparticles (Fig. 5 SOM *LPE*, inset) and showing a rough superficial mammillated topography (Braissant et al., 2003). Particles showing unusual morphologies were also observed (Fig. 5SI A). The FTIR spectra of these precipitates always showed the characteristic absorption bands of calcite (v_3 = 1420 cm^{-1}; v_2 = 875 cm^{-1}; v_4 = 712 cm^{-1}) plus additional bands (Fig. 6SI A). In the presence of *M. caliculata* SOM additional bands at 1082 cm^{-1}, 1030 cm^{-1} and 1474 cm^{-1} were observed together with a relative weakening of the band at 712 cm^{-1}. These features may agree with the co-presence of amorphous calcium carbonate (ACC) (Addadi et al., 2003). In the presence of *L. pertusa* SOM the other bands were at 1487 cm^{-1}, 1464 cm^{-1}, 1437 cm^{-1} and 744 cm^{-1}, suggesting the co-precipitation of vaterite (Table 3). In the presence of dispersed IOM (c_i = 0.625 mg/mL), that sometime floated at the air-solution interface, the deposition of mineral particles was mainly observed on the IOM surface. The FTIR spectra showed the presence of the typical absorption bands of calcite, together with those of IOM (Fig. 6SI B). Onto IOM from *M. caliculata*, *L. pertusa* or *A. digitifera* calcite crystals showing truncation of rhombohedral corners and edges (Fig. 5 IOM and insets) were observed. Rare crystals like those precipitated in presence of SOM (Fig. 5SI C) and spherulitic particles were also observed (Fig. 5SI B) with IOM form *M. caliculata* and *A. digitifera*, respectively. The co-presence of SOM (c_s) and IOM (c_i) favored the precipitation of small particles clustered into big aggregates (Fig. 5 SOM + IOM and insets). With *M. caliculata* and *A. digitifera* OM fractions the surface of the IOM was covered by particles having a rough surface formed by the aggregation of nanoparticles. In the presence of *L. pertusa* SOM and IOM particles having the shapes and the morphologies observed in the presence of the two single fractions were observed. The distribution among these shapes and morphologies changed from one experiment to another (Fig. 5 SOM + IOM and Fig. 5SI D). The FTIR spectra of these materials showed the same absorption bands observed in the presence of SOM. In the presence of *A. digitifera* SOM and IOM absorption bands (1457 and 744 cm^{-1}) associable to vaterite were also observed (Fig. 6SI C).

A second set of CaCO$_3$ precipitation experiments was conducted using a 10 mM CaCl$_2$ with Mg/Ca molar ratio equal to 3, solution to
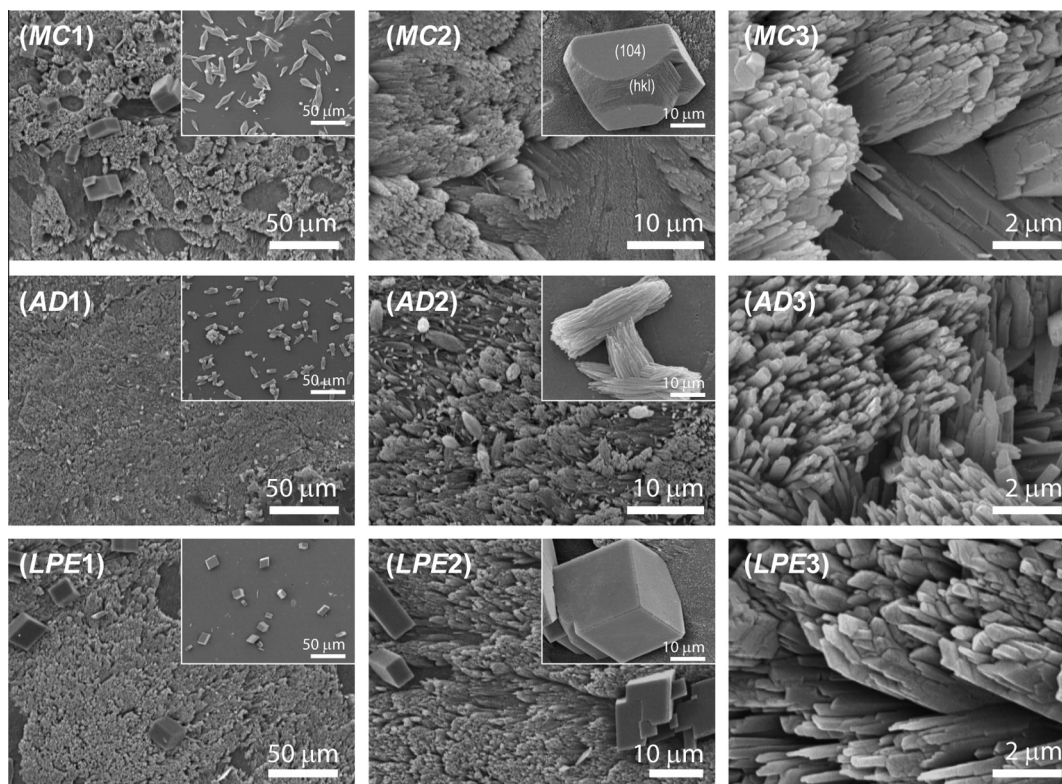
Fig.4. SEM pictures at increasing magnifications (1–3) of sections of coral skeleton of *A. digitifera* (*AD*), *L. pertusa* (*LPE*) and *M. caliculata* (*MC*) after the calcium carbonate overgrowth experiment. The insets in *AC*1, *LPE*1 and *MC*1 show the crystals precipitated outside the coral skeleton. The inset in *AD*2 shows a magnification of an aragonite crystal overgrown outside the skeleton. The insets in *LP*2 and *MC*2 show magnification of calcite crystals (over)grown on the coral skeleton section. The crystals of calcite overgrown on *M. caliculata* showed an additional {hk0} faces other than the {104} faces. These crystals also appeared outside the skeleton with the precipitated aragonite ones. Their extension was generally higher in the crystals observed on the skeleton than outside it.

which SOM, IOM or SOM plus IOM were added. The co-presence of Mg ions and OM fractions had an inhibitory effect on the precipitation process and caused, once more, variability in the $CaCO_3$ polymorphism and morphology of the precipitates (Table 2SI), the presented results reveal a general trend (Fig. 6, Table 3). In the absence of OM fractions crystals elongated along the c-axis and needle shaped crystal aggregates typical of magnesium calcite and aragonite, respectively, were observed (Fig. 4SI) together with rare botryoidal aggregates (Fig. 7SI A). The addition of c_s of SOM provoked a strong inhibition of the precipitation and only few aggregates were observed (Fig. 6 SOM and insets). The FTIR spectra of these materials showed only typical absorption bands of magnesium calcite (v_2 band at 876 cm^{-1}) and suggested the presence of ACC (very weak v_4 band at 712 cm^{-1} and splitting of the v_3 band at 1462 and 1420 cm^{-1}) (Fig. 8SI A). These aggregates showed the rod, dumbbell and, sometimes, spherical shapes, already observed in the control experiments; however, sometimes in the presence of *L. pertusa* and *A. digitifera* SOMs the particles' crystalline habits were partially or completely lost (Fig. 6 SOM *LPE* and Fig. 7SI B) and the particle surfaces were quite smooth (Fig. 6 SOM *AD*, inset). In the presence of IOM the precipitate was observed on and around it. The mineral particles appeared elongated and showed spherulitic aggregation (Fig. 6 IOM). In the presence of *A. digitifera* and *M. caliculata* IOM, and particularly of *L. pertusa* IOM, the particles observed on the IOM lose their crystalline habit (Fig. 6 IOM, Fig. 7SI C). The FTIR spectra of these materials showed the same absorption bands of magnesium calcite (875/6 cm^{-1}) and aragonite (858 cm^{-1}) observed in the absence of OM. However, in some cases the band at 858 cm^{-1} was not observed. Once more the calcitic v_4 band was very weak compared to the v_2 one (Fig. 8SI B). In the co-presence of SOM and IOM a strong inhibition of the $CaCO_3$

precipitation was observed and only few particles precipitated outside the IOM (Fig. 7SI D). In the presence of *M. caliculata* OM fractions these particles grew also on the IOM (Fig. 6 SOM + IOM MC). In the presence of *A. digitifera* and *L. pertusa* OM fractions the IOM was covered by aggregates of nanoparticles (Fig. 6 SOM + IOM *AD*, inset) and the mineral particles showed an irregular framboid spherical shape surface (Fig. 6 SOM + IOM *LPE*), respectively. The FTIR spectra of these materials showed the same pattern observed in presence of only SOM. Broad absorption bands at 1030 cm^{-1} and 1082 cm^{-1} were also present (Fig. 8SI C).

2.5. Atomic force microscopy (AFM) observations of $CaCO_3$ precipitated in the presence of OM fractions

Precipitates obtained using the OM fractions extracted from *M. caliculata*, *L. pertusa* and *A. digitifera*, with or without Mg, have been studied by AFM. Only the data related to *M. caliculata* are presented here. The shape of the mineral precipitations is better seen with SEM, but similar morphologies have been observed. The surface of the precipitates obtained with the SOM of *M. caliculata* was rough and composite in height (= morphological) images (Fig. 7a). They were probably dispersed in a thin OM. Phase images show that the elements seen in height images were composed of granules, the shape and size of which were irregular (Fig. 7b). However, the observed morphologies of these granules were not like those of purely crystalline minerals: they were devoid of angle and facets. These granules were surrounded by a more or less distinct cortex (Fig. 7b). The color of each granule is nonuniform in phase images, indicative of a heterogeneous composition. The precipitates obtained using IOM of *M. caliculata* were rhombohedral, as seen using SEM. Height images showed a layered structure with
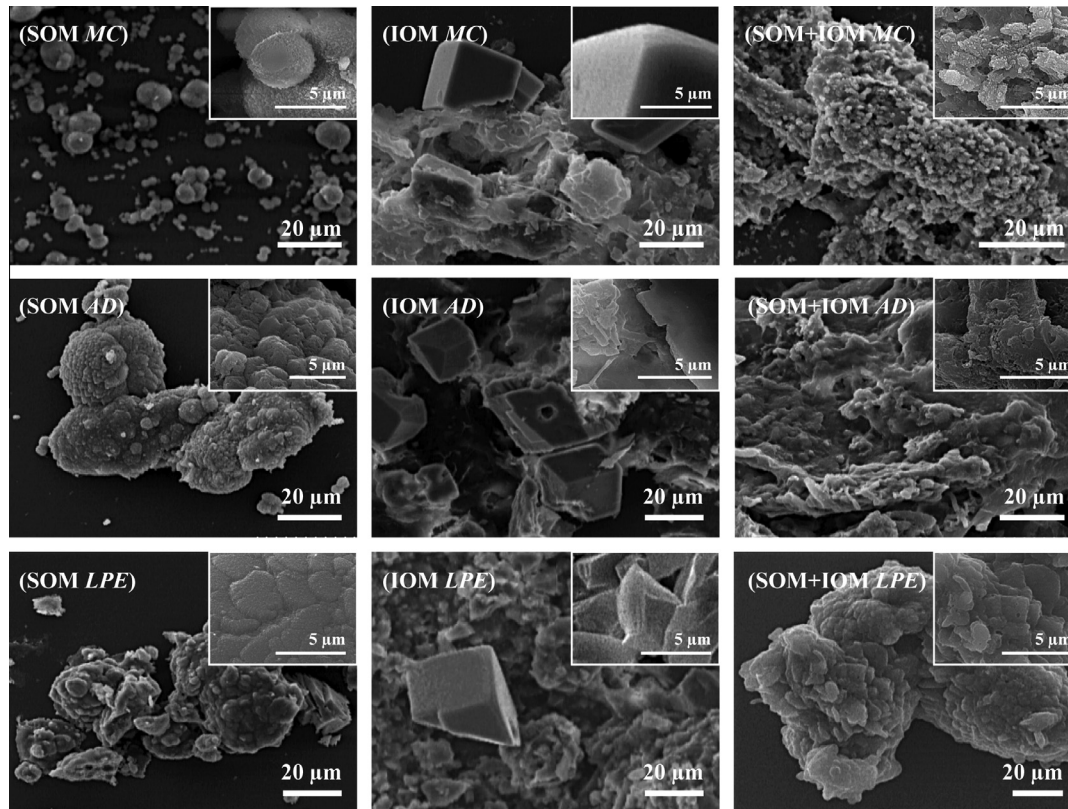
Fig.5. SEM pictures of particles obtained from precipitation experiments of CaCO$_3$ from 10 mM CaCl$_2$ solutions in the presence of OM fractions. In the first, second and third columns are shown particles obtained in the presence of SOM, IOM and SOM + IOM, respectively. The first, second and third rows refer to the extracts from, *M. caliculata* (*MC*), *A. digitifera* (*AD*) and *L. pertusa* (*LPE*), respectively. In the insets are reported high magnification pictures of the particles. The calcite crystals on IOMs showed a light truncation of rhombohedral {104} corners and edges (probably the presence of small {108} and {hk0} faces). These pictures are the most representative of the populations of observed particles.

Table 3

Features CaCO$_3$ particles precipitated in a 10 mM CaCl$_2$ solution with or without Mg ions with Mg/Ca molar ratio equal to 3 using as additives SOM (c_s = 0.44 mg/mL), IOM (c_i = 0.50 mg) or both of them, SOM (c_s) + IOM (c_i). The additives were extracted from the skeleton of *A. digitifera* (*AD*), *M. caliculata* (*MC*) and *L. pertusa* (*LPE*). When two phases were obtained the main one is indicated as first.

	Ca solution			SOM			IOM			SOM + IOM			Mg/Ca solution			SOM			IOM			SOM + IOM		
	p	s	D	p	s	d	p	s	d	p	s	d	p	s	d	P	s	d	p	s	d	p	s	d
MC	C	rh	30	C	pn, db	5	C	rh	20	C	sp	4	A	sp	45	MgC	db	4	MgC	sp	5	MgC	db	3
				ACC	nd					ACC	nd		MgC	rd	5	ACC	nd					ACC	nd	
AD	C	rh	30	C	db, sp	9	C	rh	40	C	sp	4	A	sp	45	MgC	db	6	A	sp	56	MgC	db	6
										V			MgC	rd	5	ACC	nd		MgC	rd		ACC	nd	
LPE	C	rh	30	C	sp	9	C	rh	45	C	sp	3	A	sp	45	MgC	db	3	MgC	sp	7	MgC	db	6
				V	sp					V			MgC	rd	5	ACC	nd		A	nd		ACC	nd	

C, A, V, MgC and ACC indicate calcite, aragonite, vaterite, magnesium calcite and amorphous calcium carbonate, respectively. *p*, *s* and *d* indicate phase, shape and average size along the main axis (µm) of the CaCO$_3$ precipitated particles. In the case of V and ACC the size of particles or aggregates was in a very wide range of dimensions such to make the average size not significant. In these cases is not reported. The shapes were named according to the literature (Braissant et al., 2003; Sommerdijk and de With, 2008; Meldrum and Coelfen, 2008); rh = rhombohedra; pn = peanuts; db = dumbbells; sp = spherulites, nd = not definable shape originated by the aggregation of nano-sized spherical particles.

rounded denticulate outlines (Fig. 7c). The phase image shows that the layers were not compact and they were rich in OM (in black in Fig. 7d). Again, granules within a layer are heterogeneous in composition, and irregular in shape and size. Shapes obtained using SOM and IOM differ: the units were elongated and composite (Fig. 7e, f), with nano growth lines (Fig. 7f). Rounded granules were also present. Addition of Mg to the SOM of *M. caliculata* resulted in various morphologies (Fig. 7g, h). Nevertheless, granules within these precipitates were irregular in shape and size (Fig. 7g), while the elongated units showed faint growth lines (Fig. 7h). Addition of IOM generated flat units (Fig. 7i), the inner structure of which con-

sisted of rounded granules (Fig. 7j). The mixture of SOM, IOM and Ca/Mg leads to more angular crystals (Fig. 7k), but as for the previous samples, granules were heterogeneous in composition and surrounded by a cortex (Fig. 7l).

3. Discussion

Corals challenge some widespread notions about biomineralization and the importance of OM components in promoting and organizing mineral growth. They do incorporate organic materials
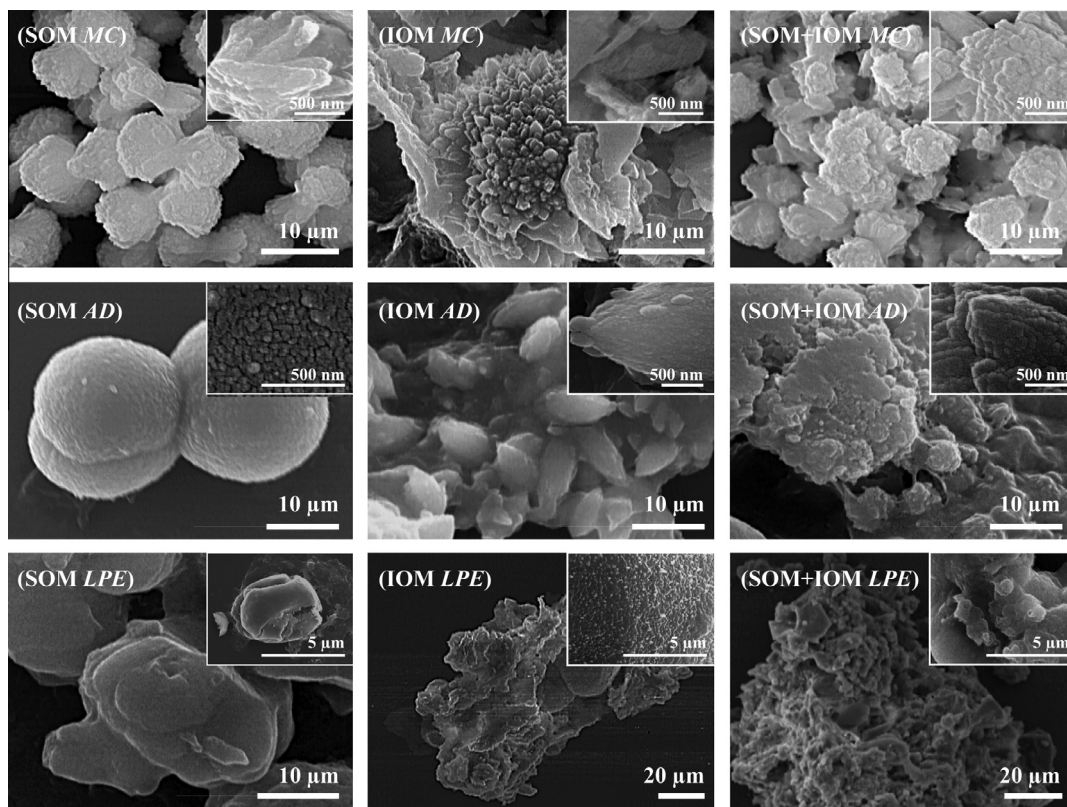
Fig.6. SEM pictures of particles obtained from precipitation experiments of CaCO$_3$ from 10 mM CaCl$_2$ solutions with Mg/Ca ratio equal 3 in the presence of OM fractions. In the first, second and third columns are shown particles obtained in the presence of SOM, IOM and SOM + IOM, respectively. The first, second and third rows refer to the extracts from *M. caliculata* (*MC*), *A. digitifera* (*AD*), and *L. pertusa* (*LPE*), respectively. In the insets are reported high magnification pictures of the particles. These pictures are the most representative of the populations of observed particles. When in the control experiments aggregates having a botryoidal texture were observed, they were also observed in the presence of *L. pertusa* IOM (Fig. 7SI C).

into their skeletons, but they do not shape or organize their skeletal crystals with anything approaching the care seen in molluscan shells (Lowenstam and Weiner, 1989; Tambutté et al., 2011). However, corals calcify a hundred times faster than inorganic calcification rates on the reef, and faster than most other animals, and thereby display a strong command over the biomineralization process (Marshall and Clode, 2004). Despite the fact that an extracellular calcification occurs outside the ectodermal cell layer, the control of skeletal organization remains an unresolved question (Goffredo et al., 2011).

In this study the skeleton from three colonial coral species, *A. digitifera*, *M. caliculata* and *L. pertusa* was used. *A. digitifera* and *M. caliculata* are tropical corals living in hot waters, while *L. pertusa* lives on the North Atlantic coast in cold waters. *A. digitifera* shows a rate of calcification higher than the other two species (Veron, 1993; De'ath et al., 2009; Takahashi and Kurihara, 2012). The skeleton of these species, as that of all corals, shows differences in the textural organization of the fibers and EMZ zone regions (Cuif et al., 1996; Cuif and Dauphin, 2005). This species specific difference comes from the coral's biological activities in which, among many processes (i.e. ion trafficking (Gagnon et al., 2012)), there is the release of the OM molecules in the confined extracellular calcification site (Allemand et al., 2011). Some of these molecules are then entrapped in the forming mineral phase, with which they interact. If these molecules are subject to re-organization (Adamiano et al., 2012), and eventually degradation, while being hosted in the mineral matrix is still unclear (Tambutté et al., 2011). It has been demonstrated that in mollusk shells the OM control on the biomineralization process requires that specific macromolecules are located in a specific gelling environment (Falini et al., 1996; Su-

zuki et al., 2009; Asenath-Smith et al., 2012). Much less information is available for corals on the mechanism of action of the OM molecules. The general features of OM from the three species of the studied corals are quite similar, but different in several aspects from those associated to mollusk shells. The OM matrix content ranges around 2.5% (*w/w*), but is lower in *A. digitifera*, in agreement with what reported for other coral species (Cuif et al., 2004). The fact that the amount of extracted OM is one order of magnitude lower, around 0.2% (*w/w*), is due to the extraction procedure, as also observed by other researchers (Puverel et al., 2005). The relative mass amount of the two fractions of OM shows a significant higher content of SOM than IOM. This, that occurs in *A. digitifera* (5 to 1) more than in *M. caliculata* (1.4 to 1) and *L. pertusa* (1.5 to 1), is not observed in mollusk shells where the IOM, which builds the scaffold on which the mineralization occurs, is the dominant fraction (Worms and Weiner, 1986). A high content of intra-crystalline SOM with respect to IOM is observed in organisms like algae, in which a lower control on the mineral deposition is present (Lowenstam and Weiner, 1989). OM from corals shows also other peculiarities. The SOM from *A. digitifera* is very rich in aspartate residues compared with other species and mollusk shells (Worms and Weiner, 1986). It was shown that aspartate sequences have an important role in the control of calcium carbonate precipitation (Elhadj et al., 2006; Stephenson et al., 2008). The IOMs are acidic (about 20 mol% of aspartate). This is unusual since the IOM is typically rich in hydrophobic residues, which also represent a significant fraction of coral IOMs (about 45 mol%). IOMs are also significantly rich in lipids, as was already reported for other coral species in the whole OM (Farre et al., 2010). Lipids could have a role in the mineralization process (Isa and Okazaki, 1987; Tester et al., 2011). Goffredo et al.
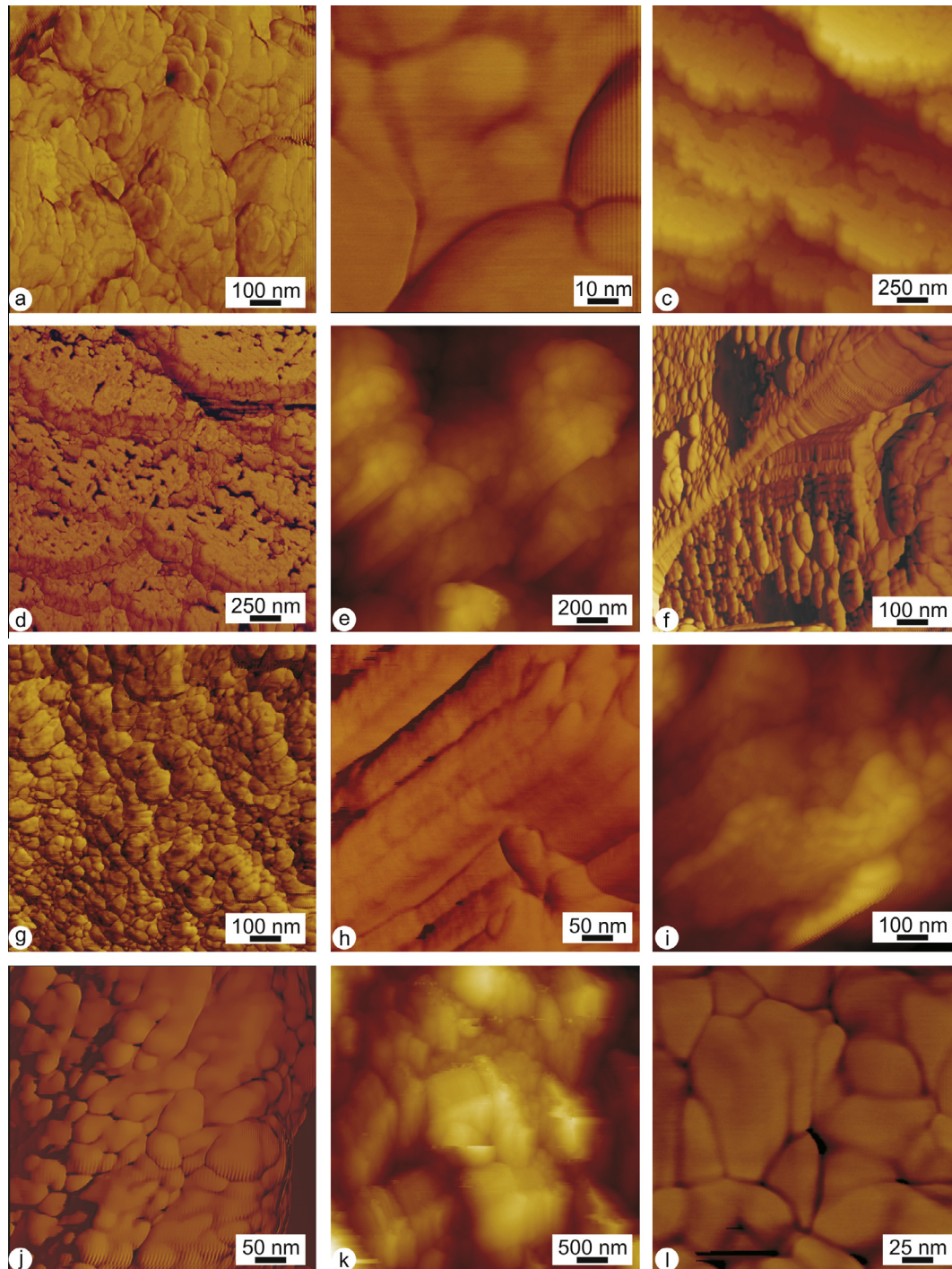
Fig.7. AFM images of crystallization experiments using OM extracted from *M. caliculata*. a–b: 10 mM CaCl$_2$ solution and SOM; irregular rounded granules; phase image. c–d: 10 mM CaCl$_2$ solution and IOM; lamellar units are a mixture of organic and minerals components as shown in phase image (d). e–f: 10 mM CaCl$_2$ solution and SOM and IOM; height image showing elongated granular units (e); phase image confirms the presence of granules and thin growth lines (f). g–h: 10 mM CaCl$_2$ solution and SOM with Mg/Ca ratio equal 3; granular structures (g) and elongated, but not flat units (h) in phase images. i–j: 10 mM CaCl$_2$ solution and IOM with Mg/Ca ratio equal 3; flat units (i, height image) are composed of round granules (j, phase image). k–l: 10 mM CaCl$_2$ solution and SOM and IOM with Mg/Ca ratio equal 3; height image showing angular shape of the precipitation (k), but the inner structure is granular without any facets (l, phase image).

(2011) observed that the OM from *B. europaea* devoid of lipids was unable to stabilize ACC. Recently, and importantly, several researchers suggested that lipids can be involved in processes of ionic trafficking (Weiner and Addadi, 2011 and references therein), although different processes were suggested to be present in corals (Gagnon et al., 2012). The conformation of proteins in SOM appears to be mainly in α-helix or random coil, while in IOM is mainly in β-

sheet. Other characterizations of coral OM, which focused only on the SOM, confirmed the absence of β-sheet conformation in it (Dauphin, 2001; Wanatabe et al., 2003; Dauphin et al., 2008). These different conformations could play a role in discriminating the molecules' aggregation and solubility (Falini et al., 2003). It was shown that in corals SOM and IOM are constituted by the same macromolecules, in the IOM richer in high molecular weight, and less

hydrophilic, than those in SOM (Goffredo et al., 2011). Thus, it cannot be excluded that the extraction procedure could be partially responsible of familiarization in SOM and IOM. The above observations narrow, at least for corals, the distinction between IOM and SOM. *A. digitifera* produces almost only SOM that does not stain bands after the SDS–PAGE, suggesting that it is composed of low molecular weight acidic molecules (pI = 3.7) very mobile (Gotliv et al., 2003) and with low tendency to aggregate and precipitate in water. SOM and IOM are both present in the OM matrix of *M. caliculata* and *L. pertusa*. These acidic IOMs have a tendency to form a gel. Very importantly it was recently demonstrated using "proto-polyp" cell cultures from *Stylophora pistillata* that the precipitation of aragonite occurs in a gel environment (Mass et al., 2011).

The capability of intra-crystalline OM molecules to influence the precipitation of $CaCO_3$ was studied both by $CaCO_3$ overgrowth on the coral skeleton sections and by $CaCO_3$ precipitation from solutions.

Overgrowth experiments allow to study specific crystal-macromolecules interactions under conditions that minimally affect the macromolecules native state (Aizenberg et al., 1994). They are certainly more conducive to preserving their structure that after isolation and separation procedures. Moreover, not all the intraskeletal macromolecules could be released by the skeletal elements. The presence of aragonite overgrowth on the coral skeleton suggests a capability of the OM components to stabilize this polymorph, even in the absence of magnesium ions. However, the possibility of a direct secondary nucleation on aragonite cannot be excluded, unless aragonite was observed as unique phase outside the skeleton. Aragonite was likewise observed in the precipitate as the unique phase when *A. digitifera* skeleton was used. This observation can be related to the peculiar features of the OM of *A. digitifera* described above. On the surface of *M. caliculata* and *L. pertusa* was observed the co-presence of calcite crystals, as well on the surrounding of the skeleton. In *L. pertusa* calcite crystals growth was not affected by the OM molecules and they showed only the cleavage {104} faces of calcite. This was not the case of the ones that grew on the skeleton of *M. caliculata*, where additional {hk0} faces developed as a result of selective re-adsorption of the soluble macromolecules released from the coral skeleton (Addadi et al., 2006). The higher expression of the {hk0} faces in the crystals on the skeleton with respect to those outside it, could be related to the diffusion process of the macromolecules. In *M. caliculata* aragonite precipitation was observed also outside the skeleton. These divergent results have to be related to the release of different OM molecules from diverse skeletons species. Indeed, different distributions of families of molecules were observed (see FTIR, AAA and SDS–PAGE data).

Calcium carbonate precipitation experiments were also conducted to evaluate the SOM and IOM fractions influence on the calcification process (Table 3). This was done using an *in vitro* assay (Addadi et al., 1987) far from the real biological environment, but able to simulate the mineralization process by increasing concentration of carbonate ions. In the absence of magnesium ions, and in the presence of the OM fractions, the precipitation of calcite was always observed. The presence of SOM stabilized also the precipitation of ACC and vaterite in *M. caliculata* and *L. pertusa*, respectively. The SOM from *A. digitifera*, once more, acted diversely having no effect on the polymorphism of $CaCO_3$ (i.e. only calcite precipitated). However, in this set of experiments the main effect of OM fractions was on the precipitate's morphology. Aggregates of calcite particles having the shape of dumbbells, rods and peanuts (Sommerdijk and de With, 2008; Meldrum and Coelfen, 2008) were observed in the presence of the SOM from all the species. These aggregates always appeared to be formed by the assembly of sub micron sized particles, and the AFM observations showed that they were covered by an organic shell. The granular structure suggests that their precipitation occurred by a non-classical mechanism in

which the precipitation took place by the assembly of preformed units (Kulak et al., 2007; Song et al., 2009). Indeed, the coral skeleton is composed of nanosized grains (Cuif et al., 2008; Motai et al., 2012). The precipitation of these particles may occur through a transient ACC phase under conditions of high supersaturation (Kulak et al., 2007; Song et al., 2009). Accordingly, the presence of SOM from *M. caliculata* seems to stabilize ACC.

In the magnesium ions free $CaCO_3$ precipitation experiments aragonite was observed only when few components of the SOM were released in solution (i.e. overgrowth experiments), but not when all the extracted components of the OM were in solution. It should be also considered that in the extraction procedure the low molecular weight (MW < 3500 Da) molecules are lost, and they could have a role in the control of the precipitation process. Moreover, in corals, the calicoblasts express and secret in the nucleation site the OM molecules at different times and spaces. Thus, the use of all the extracted intra-crystalline molecules, considering the denaturation associated to the extraction process, could bring to lower level of polymorphism control on the precipitation of $CaCO_3$ *in vitro*. However, these molecules influence the morphology of the precipitating phase.

The presence of magnesium ions in the extracytoplasmic calcifying fluid, at the nucleation site of corals, has been reported (Holcomb et al., 2009; Tambutté et al., 2012). The analysis of the results of the $CaCO_3$ precipitation in the presence of magnesium ions and OM fractions show, differently from what observed in their absence, a strong effect on the polymorphism and a lower effect on the morphology of the precipitated particles. While in the control experiments the co-precipitation of magnesium calcite and aragonite was observed in the presence of SOM from all the species the precipitation of aragonite was inhibited and that of ACC favored. Magnesium ions have an inhibitory effect on the precipitation of $CaCO_3$, while they stabilize ACC in the presence of additives (Weiss et al., 2002; Addadi et al., 2003). As a seemingly opposite effect, magnesium ions favor the precipitation of aragonite (Lipmann, 1973; Falini et al., 2009; Tao et al., 2009). This apparent dichotomy could be explained by considering the role of OM components. Some of these components having strong affinity for aragonite (they are in an aragonitic skeleton) could interact with the aragonite nuclei inhibiting their growth, favoring the precipitation of other phases, and changing the final crystal's shape. Thus, from these observations it seems that magnesium ions, together with some specific OM molecules, could play also important roles in the control of fibers' shape (i.e. fibers length) in the coral skeleton (Cuif et al., 2008).

4. Conclusions

This work on the intra-crystalline OM from *M. caliculata*, *A. digitifera* and *L. pertusa*, and its influence of the precipitation of $CaCO_3$ shows that (*i*) among species the OM has similar chemical features that differs from that from mollusk shell; (*ii*) the OM from *A. digitifera* appears more acidic and formed by a family of more soluble small molecules which are less prone to aggregate with respect to those from *M. caliculata* and *L. pertusa*; (*iii*) OM molecules of *A. digitifera* are able to induce the deposition only of aragonite in $CaCO_3$ overgrowth experiments; (*iv*) in the presence of OM fractions and magnesium ions the SOM inhibits the precipitation of aragonite and induces changes in the morphology of calcite, which are species specific; (*v*) the peculiarity OM molecules from *A. digitifera* could be involved in the control of the high calcifying rate of this species. Thus, based on our results we may safely conclude that the OM components and magnesium ions influence, in species specific way, the fine scale characteristics of the crystals of which the coral skeleton is constructed.

5. Methods and materials

5.1. Coral skeletons

Samples of *M. caliculata* and *A. digitifera* from Mangareva atoll (French Polynesia) were collected by SCUBA diving and of *L. pertusa* from Bay of Biscay (French coast, Atlantic Ocean) by deep-sea dredging. After collection the corals were dipped in a sodium hypochlorite solution (commercial), changed every 4 days, until the polyp tissue was completely dissolved. Each skeleton was analyzed under a binocular microscope to remove fragments of substratum and calcareous deposits produced by other organisms. Subsequently, the skeletons were ground in a mortar to a fine and homogeneous powder. The powder was suspended (1% w/v) in a sodium hypochlorite solution (2.5% v/v) to remove any traces of organic material not removed by the first treatment, the cleansed powder was washed with milli-Q water (resistivity 18.2 MΩ cm at 25 °C; filtered through a 0.22 μm membrane) and dried in an oven at 37 °C for 24 h. X-ray powder diffraction patterns of the skeleton were collected using a PanAnalytical X'Pert Pro equipped with X'Celerator detector powder diffractometer using Cu Kα radiation generated at 40 kV and 40 mA. The diffraction patterns were collected within the 2Θ range from 10° to 60° with a step size (Δ2Θ) of 0.02° and a counting time of 1200 s. An estimation of the organic matter content in the coral was determined by thermo-gravimetric analysis (TGA) on a SDT Q600 simultaneous thermal analysis instrument (TA instrument). The analysis was performed under nitrogen flow from 30 to 120 °C with a heating rate of 10 °C min⁻¹, an isothermal at 120 °C for 5 min, and another cycle from 120 to 600 °C with the same heating rate.

5.2. Extraction of the organic components

Five milliliter of milli-Q water, in which 2.5 g of powdered coral skeleton were dispersed, were poured into a 40 cm-long osmotic tube for dialysis (MWCO = 3.5 kDa; CelluSep®, MFPI). The sealed tube was put into 1 L of 0.1 M CH₃COOH (Riedel–de Haen) solution under stirring. The decalcification proceeded for 72 h. At the end the tube containing the dissolved OM was dialysed against milli-Q water until the final pH was about 6. The obtained aqueous solution containing the OM was centrifuged at 350g for 5 min to separate the soluble (SOM) and the insoluble (IOM) OM fractions, which were then lyophilized and weighed. The content of OM in the skeleton was gravimetrically determined.

5.3. Characterization of the organic matrix

SDS–PAGE was performed on 12.5% polyacrylamide gel in a vertical slab gel apparatus (Mini-PROTEAN®, Bio-Rad). For these analyses only the SOM solution before the lyophilization was utilized. It was filtered and concentrated through Centricon® YM-3 (Amicon, cutoff 3 kDa) to a final volume of 1 mL. Different sample volumes were applied to the gel lanes (10, 15, 20 μL). Samples were prepared adding reduced sample buffer 1X (60 mM Tris–HCl pH 6.8; 2% SDS; 2.5% β-mercaptoethanol; 10% glycerol; 0.025% bromophenol blue) and then boiled at 100 °C for 5 min. The gels ran at constant voltage of 100 V for 1.5 h at room temperature. Proteins were detected with silver nitrate as the staining agent. These proteins may have a pronounced tendency to diffuse out of the gel because they are very acidic; therefore, the gel was immersed in different fixing solutions that involved the simultaneous use of two reagents, formaldehyde and glutaraldehyde, to trap the proteins in the gel before staining. To observe the presence of glycoprotein the PAS (Periodic Acid Schiff) stain was applied. Aminoacid analysis was conducted by a chromatographic technique using an amino acid analyzer. The OM material was weighed, then hydrolyzed at 100 °C for 24 h in 6 M HCl vapor, and analyzed using a Dionex BIOLC amino acid analyzer. Lyophilized IOM and SOM were hydrolyzed with 6N HCl for 24 h at 110 °C. During hydrolysis, complete or partial destruction of several amino acids occurs: tryptophan is destroyed; serine and threonine are partially destroyed. Sulphur amino acids are altered. Amino acid composition of the hydrolysates was also determined by high performance liquid chromatography (HPLC) using pre-column derivatization with ortho-phtalaldehyde (OPA) for primary amines and fluorometric detection. Fluorescence intensity of OPA-derivatized amino acids was monitored with an excitation wavelength of 330 nm and an emission wavelength of 450 nm.

Spectroscopic Fourier transform infrared (FTIR) analyses were conducted by using a FTIR Nicolet 380 Thermo Electron Corporation, working in the range of wave-numbers 4000–400 cm⁻¹ at a resolution of 2 cm⁻¹. Disk was obtained mixing a small amount (<1 mg) of SOM or IOM with 100 mg of KBr and applying a pressure of 48.6 tsi (670.2 MPa) to the mixture using a hydraulic press. Aminoacid analyses and FTIR spectra results were submitted to a statistical analysis with Mann–Whitney test.

5.4. CaCO₃ overgrowth experiments

Transversal sections of coral skeletons were placed in a microplate for cellular culture (MICROPLATE 24 well with Lid, IWAKI) or in a Petri dish (d = 3.2 cm) according to the size of different skeletons. The specimens were overlaid with 750 μL or 3360 μL of 10 mM CaCl₂ solution respectively. CaCO₃ crystals were grown for four days. The overgrown specimens were then lightly rinsed with milli-Q water, dried and examined in the scanning electron microscope (SEM) after coating with gold.

5.5. CaCO₃ crystallization experiments

A $30 \times 30 \times 50$ cm³ crystallization chamber was used. Two 25 mL beakers half-full of $(NH_4)_2CO_3$ (Carlo Erba) and two Petri dishes (d = 8 cm) full of anhydrous CaCl₂ (Fluka) were placed inside the chamber. Microplates for cellular culture (Microplate 24 well with Lid, IWAKI) containing a round glass cover slip in each well were used. Into each well, 750 μL of 10 mM CaCl₂ solutions having Mg/Ca ratio equal to 0 or 3 (CaCl₂.2H₂O, Merck; MgCl₂.6H₂O, Sigma–Aldrich) were poured. Eight microlitre (for *L. pruvoti*) or 20 μL (for *M. caliculata* or *L. pertusa*) of a solution obtained dissolving lyophilized SOM in water (17.5 mg/mL (hereafter reported as c_s) were added to 750 μL of 10 mM CaCl₂ solution (without or with magnesium ions). This quantity was chosen keeping in consideration the SOM concentration in the native skeleton and on the base of the experience from previous work carried out in our lab (Goffredo et al., 2011). In a second set of experiments 0.5 mg of IOM (hereafter reported as c_i) were added to 750 μL of 10 mM CaCl₂ solution (without or with magnesium ions). SOM (c_s) and the IOM (c_i) were added to each well in a third set of experiments. The micro-plate was covered with aluminum foil and a hole was made over every well. After 4 days the crystals were washed three times with milli-Q water and then analyzed. All the experiments were conducted at room temperature. The crystallization tests of CaCO₃ in the different conditions were replicated six times, starting from different batches of OM fractions (see Table 2SI).

5.6. Microscopic observations

SEM: several fractured and polished sections of coral skeletons were cut perpendicular and parallel to the surface of the septa and walls. Polished sections and some fractures were etched with various acids and enzymes to reveal microstructural features. Detailed

procedures of sample preparation are given in the legend of figures. SEM observations were conducted using a Philips XL30 at IDES laboratory (Université Paris-Sud) and a Phenom Pro-X (FEI). The optical microscope observations of $CaCO_3$ precipitates were made with a Leica microscope equipped with a digital camera. The SEM observations were conducted in a scansion electronic microscope using a Phenom™ microscope (FEI) for uncoated samples and a Hitachi FEG 6400 microscope for samples after coating with gold.

AFM: AFM observations were obtained with a Dimension 3100 Nanoscope III (Veeco Instruments) housed at UMR IDES. Samples were imaged at room temperature and in air using tapping mode. In phase imaging, a variant of tapping mode, the phase lag of the cantilever oscillation relative to the signal sent to the cantilever's piezo driver is used as a basis for image generation. Phase images were generated as a consequence of variations in material properties such as composition, adhesion, friction, etc. Thus, understanding of the contribution of the individual factors to the phase shift is not simple. Despite the complications involved in interpretation, phase contrast is a commonly used technique for mechanical and composition characterization of sample surfaces. In organo-mineral samples such as biominerals, a detailed interpretation of phase image is not possible. The probe consists of a cantilever with an integrated silicon nitride tip (Digital Instruments).

AFM has several advantages over most SEM, e.g., samples do not require coating. However, disadvantages are the small image size and a reduced depth of field on the order of micrometers. Thus, observation of fractured surfaces is difficult, and most samples have to be polished and cleaned. Depending upon the structures of the coral skeletons, different preparative processes were used (see details in the legends). $CaCO_3$ precipitates were dried in open air on a glass support and observed without any further preparation.

FTIR spectra of $CaCO_3$ samples in KBr disks were collected as reported for OM fractions.

Acknowledgments

Appendix A. Supplementary data

Supplementary data associated with this article can be found, in the online version, at http://dx.doi.org/10.1016/j.jsb.2013.05.001.

References

Adamiano, A., Bonacchi, S., Calonghi, N., Fabbri, D., Falini, G., et al., 2012. Structural changes in a protein fragment from abalone shell during calcium carbonate precipitation. Chem. Eur. J. 18, 14367–14374.

Addadi, L., Moradian, J., Shay, E., Maroudas, N.G., Weiner, S., 1987. A chemical model for the cooperation of sulfates and carboxylates in calcite crystal nucleation: relevance to biomineralization. Proc. Natl. Acad. Sci. U.S.A. 84, 2732–2736.

Addadi, L., Raz, S., Weiner, S., 2003. Taking advantages of disorder: amorphous calcium carbonate and its role in biomineralization. Adv. Mater. 15, 959–970.

Addadi, L., Joester, D., Nudelman, F., Weiner, S., 2006. Mollusk shell formation: source of new concepts for understanding biomineralization processes. Chem. Eur. J. 12, 981–987.

Adkins, J.F., Boyle, E.A., Curry, W.B., Lutringer, A., 2003. Stable isotopes in deep-sea corals and a new mechanism for "vital effects". Geochim. Cosmochim. Acta 67, 1129–1143.

Aizenberg, J., Albeck, S., Weiner, S., Addadi, L., 1994. Crystal-protein interactions studied by overgrowth of calcite on biogenic skeletal elements. J. Cryst. Growth 142, 156–164.

Allemand, D., Tambutté, É., Zoccola, D., Tambutté, S., 2011. Coral calcification, cells to reefs. In: Dubinsky, Z., Stambler, N. (Eds.), Coral reefs: an ecosystem in transition. Part III, pp. 119–150.

Asenath-Smith, E., Li, H., Keene, E.C., Wei Seh, Z., Estroff, L.A., 2012. Crystal growth of calcium carbonate in hydrogels as a model of biomineralization. Adv. Funct. Mater. 22, 2891–2914.

Braissant, O., Cailleau, G., Dupraz, C., Verrecchia, E.P., 2003. Bacterially induced mineralization of calcium carbonate in terrestrial environments: The role of exopolysaccharides and amino acids. J. Sediment. Res. 73, 485–490.

Bryan, W.H., Hill, D., 1941. Spherulitic crystallization as a mechanism of skeletal growth in the hexacorals. Proc. R. Soc. Qld. 52, 78–91.

Clode, P.L., Marshall, A.T., 2002. Low temperatures FESEM of the calcifying interface of a scleractinian coral. Tissue Cell 34, 187–198.

Cohen, A.L., McConnaughey, T.A., 2003. Geochemical perspectives on coral mineralization. In: Dove, P.M., Weiner, S., Yoreo, J.J. (Eds.), Biomineralization, Rev. Mineral Geochim., pp. 151–187.

Constantz, B., Weiner, S., 1988. Acidic macromolecules associated with the mineral phase of scleractinian coral skeletons. J. Exp. Zool. 248, 253–258.

Cuif, J.-P., Dauphin, Y., Denis, A., Gautret, P., Marin, F., 1996. The organo-mineral structure of coral skeletons: a potential source of new criteria for scleractinian taxonomy. Bull. Inst. Oceanogr. Monaco 14 (4), 359–367.

Cuif, J.-P., Dauphin, Y., 1998. Microstructural and physico-chemical characterization of 'centers of calcification' in septa of some recent scleractinian corals. Paläontol. Z. 72, 257–270.

Cuif, J.-P., Lecointre, G., Perrin, C., Tillier, A., Tillier, S., 2003a. Patterns of septal biomineralization in scleractinia compared with their 28S rRNA phylogeny: a dual approach for a new taxonomic framework. Zool. Scr. 32, 459–473.

Cuif, J.-P., Dauphin, Y., Doucet, J., Salomé, M., Susini, J., 2003b. XANES mapping of organic sulfate in three scleractinian coral skeletons. Geochim. Cosmochim. Acta 67 (1), 75–83.

Cuif, J.-P., Dauphin, Y., Berthet, P., Jegoudez, J., 2004. Associated water and organic compounds in coral skeletons: quantitative thermogravimetry coupled to infrared absorption spectrometry. Geochem. Geophys. Geosyst. 5, Q11011.

Cuif, J.-P., Dauphin, Y., 2005. The two-step mode of growth in the scleractinian coral skeletons from the micrometre to the overall scale. J. Struct. Biol. 150, 319–331.

Cuif, J.-P., Dauphin, Y., Farre, B., Nehrke, G., Nouet, J., 2008. Distribution of sulphated polysaccharides within calcareous biominerals suggests a widely shared two-step crystallization process for the microstructural growth units. Mineral. Mag. 72, 233–237.

Dauphin, Y., 2001. Comparative studies of skeletal soluble matrices in scleractinian corals and mollusks. Int. J. Biol. Macromol. 28, 293–304.

Dauphin, Y., Cuif, J.-P., Williams, C.T., 2008. Soluble organic matrices of aragonitic skeletons of Merulinidae (Cnidaria, Anthozoa). Comp. Biochem. Physiol. B 150, 10–22.

De'ath, G., Lough, J.M., Fabricius, K.E., 2009. Declining coral calcification on the great barrier reef. Science 323, 116–119.

Elhadj, S., Salter, A., Wierzbicki, A., De Yoreo, J.J., Han, N., et al., 2006. Polyaspartate chain length as a stereochemical switch for control of calcite growth and morphology. Cryst. Growth Des. 6, 197–201.

Falini, G., Albeck, S., Weiner, S., Addadi, L., 1996. Control of aragonite or calcite polymorphism by mollusk shell macromolecules. Science 271, 67–69.

Falini, G., Weiner, S., Addadi, L., 2003. Chitin–silk fibroin interactions: relevance to calcium carbonate formation in invertebrates. Calcif. Tissue Int. 72, 548–554.

Falini, G., Fermani, S., Tosi, G., Dinelli, E., 2009. Calcium carbonate morphology and structure in the presence of sea water ions and humic acids. Cryst. Growth Des. 9, 2065–2072.

Farre, B., Cuif, J.-P., Dauphin, Y., 2010. Occurrence and diversity of lipids in modern coral skeleton. Zoology 113, 250–257.

Gagnon, A.C., Adkins, J.F., Erez, J., 2012. Seawater transport during coral biomineralization. Earth Planet. Sci. Lett. 329–330, 150–161.

Goffredo, S., Vergni, P., Reggi, M., Caroselli, E., Sparla, F., et al., 2011. The organic matrix influences precipitation of skeletal calcium carbonate in the Mediterranean coral (Balanophyllia europaea). PLoS One 6, e22338.

Gotliv, B.-A., Addadi, L., Weiner, S., 2003. Mollusk shell acidic proteins: in search of individual functions. Eur. J. Chem. Biol. 4, 522–529.

Holcomb, M., Cohen, A.L., Gabitov, R.I., Hutter, J.L., 2009. Compositional and morphological features of aragonite precipitated experimentally from seawater and biogenically by corals. Geochim. Cosmochim. Acta 73, 4166–4179.

Isa, Y., Okazaki, M., 1987. Some observations on the Ca^{2+}-binding phospholipids from scleractinian coral skeletons. Comp. Biochem. Physiol. B 87, 507–512.

Jokiel, P.L., 1978. Effects of water motion on reef corals. J. Exp. Mar. Biol. Ecol. 35, 87–97.

Kulak, A.N., Iddon, P., Li, Y., Armes, S.P., Cölfen, H., et al., 2007. Continuous structural evolution of calcium carbonate particles: a unifying model of copolymer-mediated crystallization. J. Am. Chem. Soc. 129, 3729–3736.

Lipmann, F., 1973. Sedimentary carbonate minerals. Springer-Verlag, Berlin.

Lowenstam, H.A., Weiner, S., 1989. On Biomineralization. Oxford University Press, Oxford, New York.

Marshall, A.T., Clode, P., 2004. Calcification rate and the effect of temperature in a zooxanthellate and an azooxanthellate scleractinian reef coral. Coral Reefs 23, 218–224.

Mass, T., Drake, J.L., Haramaty, L., Rosenthal, Y., Schofield, O.M.E., et al., 2011. Aragonite precipitation by "Proto-Polyps" in coral cell cultures. PLoS One 7, e35049.

McConnaughey, T.A., Whelan, J.F., 1997. Calcification generates protons for nutrient and bicarbonate uptake. Earth Sci. Rev. 42, 95–117.

Meldrum, F.C., Coelfen, H., 2008. Controlling mineral morphologies and structures in biological and synthetic systems. Chem. Rev. 108, 4332–4342.

Mitterer, R.M., 1978. Amino acid composition and metal binding capability of the skeletal protein of corals. Bull. Mar. Sci. 28, 173–180.

Motai, S., Nagai, T., Sowa, K., Watanabe, T., Hisayoshi Yurimoto, S.N., 2012. Needle-like grains across growth lines in the coral skeleton of Porites lobata. J. Struct. Biol. 180, 389–393.

Ogilvie, M.M., 1896. Microscopic and systematic study of madreporarian types of corals. Philos. Trans. R. Soc. London B 187, 83–345.

Parker, F.S., 1983. Application of Infrared Spectroscopy in Biochemistry, Biology and Medicine. Plenum-Press, New York, pp. 601–625.

Puverel, S., Tambutté, E., Periera-Mouriès, L., Zoccola, D., Allemand, D., et al., 2005. Soluble organic matrix of scleractinian corals: partial and comparative analysis. Comp. Biochem. Physiol. 150B, 10–22.

Sillero, A., Ribeiro, J.M., 1989. Isoelectric points of proteins: theoretical determination. Anal. Biochem. 179, 319–325.

Sommerdijk, N.A.J., de With, G., 2008. Biomimetic $CaCO_3$ mineralization using designer molecules and interfaces. Chem. Rev. 108, 4499–4550.

Song, R.-Q., Cölfen, H., Xu, A.-W., Hartmann, J., Antonietti, M., 2009. Polyelectrolyte-directed nanoparticle aggregation: systematic morphogenesis of calcium carbonate by nonclassical crystallization. ACS Nano 3, 1966–1978.

Spalding, M.D., Ravilious, C., Green, E.P., 2001. World Atlas of Coral Reefs. University of California Press, Berkeley, 424 pp..

Stephenson, E., DeYoreo, J.J., Wu, K.J., Hoyer, J., Dove, P.M., 2008. Peptides enhance magnesium signature in calcite: insights into origins of vital effects. Science 322, 724–727.

Suzuki, M., Saruwatari, K., Kogure, T., Yamamoto, Y., Nishimura, T., et al., 2009. An acidic matrix protein, Pif, is a key macromolecule for nacre formation. Science 325, 1388–1390.

Takahashi, A, Kurihara, H., 2012. Ocean acidification does not affect the physiology of the tropical coral Acropora digitifera during a 5-week experiment. Coral Reefs (online). http://dx.doi.org/10.1007/s00338-012-0979-8.

Tambutté, S., Holcomb, M., Ferrier-Pages, C., Reynaud, S., Tambutté, E., et al., 2011. Coral biomineralization: from the gene to the environment. J. Exp. Mar. Biol. Ecol. 408, 58–78.

Tambutté, E., Tambutté, S., Segonds, N., Zoccola, D., Venn, A.A., et al., 2012. Calcein labelling and electrophysiology: insights on coral tissue permeability and calcification. Proc. Biol. Sci. 7, 19–27.

Tao, J., Zhou, D., Zhang, Z., Tang, R., 2009. Magnesium-aspartate-based crystallization switch inspired from shell molt of crustacean. Proc. Natl. Acad. Sci. U.S.A. 106, 22096–22101.

Tester, C.C., Brock, R.E., Wu, C.H., Krejci, M.R., Weigand, S., et al., 2011. In vitro synthesis and stabilization of amorphous calcium carbonate (ACC) nanoparticles within liposomes. CrystEngComm 13, 3975–3978.

Veron, J.E.N., 1993. Corals of Australia and the indo-pacific. University of Hawai Press, Honolulu.

Veron, J.E.N., 2000. Corals of the World. Austr. Inst. Mar. Sci. 1, Townsville.

Wanatabe, T., Fukuda, I., China, K., Isa, Y., 2003. Molecular analyses of protein components of the organic matrix in the exoskeleton of two scleractinian coral species. Comp. Biochem. Physiol. 136B, 767–774.

Weiner, S., Addadi, L., 2011. Crystallization pathways in biomineralization. Annu. Rev. Mater. Res. 41, 21–40.

Weiss, I.M., Tuross, N., Addadi, L., Weiner, S., 2002. Mollusc larval shell formation: amorphous calcium carbonate is a precursor phase for aragonite. J. Exp. Zool. 293, 478–491.

Wells, J.W., 1956. Scleractinia. In: Moore, R.C. (Ed.), Treatise on Invertebrate Paleontology. Part F (Coelenterata). The University of Kansas Press, Lawrence, KS, pp. F328–F344.

Wilfert, M., Peters, W., 1969. Vorkommen von Chitin bei Couelenteraten. Z. Morph. Tiere 6, 77–84.

Worms, D., Weiner, S., 1986. Mollusk shell organic matrix: fourier transform infrared study of the acidic macromolecules. J. Exp. Zool. 237, 11–20.

Young, S.D., 1971. Organic material from scleractinian coral skeletons. I. Variation in composition between several species. Comp. Biochem. Physiol. B 40, 113–120.